WATER RESOURCES RESEARCH, VOL. 39, NO. 12, 1330, doi:10.1029/2003WR002185, 2003

Water table waves in an unconfined aquifer: Experiments and modeling

Nick Cartwright, Peter Nielsen, and Scott Dunn[1]

School of Engineering, University of Queensland, Brisbane, Queensland, Australia

Received 17 March 2003; revised 21 August 2003; accepted 1 October 2003; published 3 December 2003.

[1] Comprehensive measurements are presented of the piezometric head in an unconfined aquifer during steady, simple harmonic oscillations driven by a hydrostatic clear water reservoir through a vertical interface. The results are analyzed and used to test existing hydrostatic and nonhydrostatic, small-amplitude theories along with capillary fringe effects. As expected, the amplitude of the water table wave decays exponentially. However, the decay rates and phase lags indicate the influence of both vertical flow and capillary effects. The capillary effects are reconciled with observations of water table oscillations in a sand column with the same sand. The effects of vertical flows and the corresponding nonhydrostatic pressure are reasonably well described by small-amplitude theory for water table waves in finite depth aquifers. That includes the oscillation amplitudes being greater at the bottom than at the top and the phase lead of the bottom compared with the top. The main problems with respect to interpreting the measurements through existing theory relate to the complicated boundary condition at the interface between the driving head reservoir and the aquifer. That is, the small-amplitude, finite depth expansion solution, which matches a hydrostatic boundary condition between the bottom and the mean driving head level, is unrealistic with respect to the pressure variation above this level. Hence it cannot describe the finer details of the multiple mode behavior close to the driving head boundary. The mean water table height initially increases with distance from the forcing boundary but then decreases again, and its asymptotic value is considerably smaller than that previously predicted for finite depth aquifers without capillary effects. Just as the mean water table over-height is smaller than predicted by capillarity-free shallow aquifer models, so is the amplitude of the second harmonic. In fact, there is no indication of extra second harmonics (in addition to that contained in the driving head) being generated at the interface or in the interior. *INDEX TERMS:* 1832 Hydrology: Groundwater transport; 1829 Hydrology: Groundwater hydrology; 1866 Hydrology: Soil moisture; 1875 Hydrology: Unsaturated zone; *KEYWORDS:* oscillating water table, finite depth aquifer, capillarity, effective porosity

Citation: Cartwright, N., P. Nielsen, and S. Dunn, Water table waves in an unconfined aquifer: Experiments and modeling, *Water Resour. Res.*, *39*(12), 1330, doi:10.1029/2003WR002185, 2003.

1. Introduction

[2] The availability of fresh groundwater on islands and in coastal areas in general is influenced by the nearby ocean, estuary or tidal rivers. Hence our ability to utilize many fresh water resources relies on our understanding of the interaction between neighboring tidal waters and the aquifer. The interaction between oscillating reservoirs and aquifers has therefore been the subject of experimental and theoretical research for many decades. It turns out that the groundwater dynamics in real world scenarios deviate significantly from the simplest theories, i.e., those based on the Dupuit-Forchheimer assumptions for shallow aquifers, small-amplitude oscillations and neglecting any influence from the partly saturated zone above the water table.

[3] Such deviations are best illustrated using the water table wave number which provides a description of the waves' dispersive properties. The wave number is complex in nature, $k = k_r + ik_i$, with k_r representing the amplitude decay and k_i representing the rate of increase in phase lag as the wave propagates into the aquifer. The simple, shallow aquifer, capillary free theory predicts the wave number to have equal real and imaginary parts, $k_r/k_i = 1$, whereas field observations indicate otherwise. *Nielsen* [1990] found $k_r/k_i \approx 1.7$ and *Aseervatham* [1994] found values in the range $0.7 < k_r/k_i < 2.7$. Hele-Shaw cell experiments by *Nielsen et al.* [1997] also show that $k_r/k_i > 1$.

[4] Quite a few comprehensive field data sets exist [e.g., *Nielsen*, 1990; *Kang et al.*, 1994; *Raubenheimer et al.*, 1999]. However, with all field data, the amount of complicating details in the geometry and composition of the aquifer and in the periodic forcing prevent detailed analysis of "what is due to what", i.e., which of the deviations from simple theory are caused by aquifer geometry and stratification, which are caused by capillary effects, which by

[1]Now at HR Wallingford Ltd, Howbery Park, Wallingford, UK.

0043-1397/03/2003WR002185

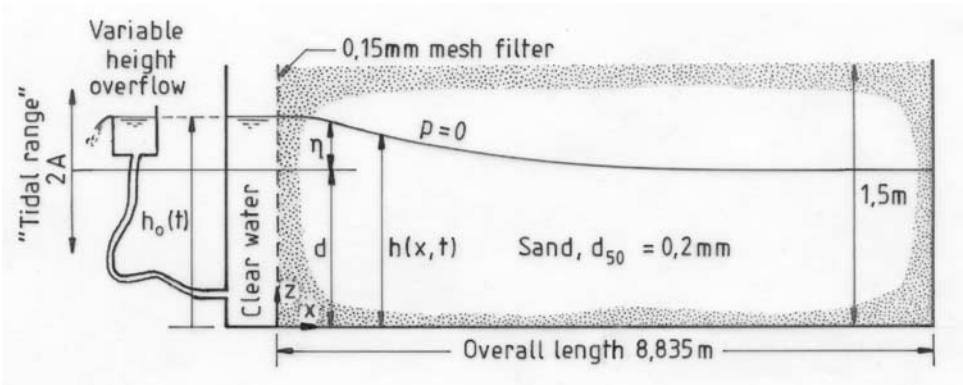

Figure 1. Experimental setup: the groundwater flow in a uniform aquifer of simple rectangular shape is driven by a simple harmonic driving head at $x = 0$ with $d = 1.094$ m, $R_\omega = 0.235$ m and $T = 772$ s. Capillary effects are significant and the aquifer is not shallow.

finite amplitude, which by vertical flows, etc. Hence the purpose of the present investigation is to provide a simple aquifer of constant depth and packing (to the extent that this is achievable) with a simple harmonic driving head acting on a vertical interface (Figure 1). Still, strong effects of finite aquifer depth and of the capillary fringe are present and enable evaluation of existing theory and identification of the most pressing issues for future research.

[5] The paper is organized as follows. Section 2 describes the experimental setup and procedures. The results are then analyzed and compared with existing theory in section 3, and the main conclusions are drawn in section 4.

2. Experimental Setup and Procedure

2.1. Flume

[6] The sand flume shown in Figure 1 is 9 m long by 14 cm wide by 1.5 m high. The flume is full to the top with sand except for a 15 cm wide, driving head reservoir at one end. A vertical stainless steel wire mesh with 0.15 mm openings (supported by a coarser grid with 2 cm openings) separates the sand from the clear water over the full depth at $x = 0$. The driving head level is regulated by a variable height overflow delivering almost simple harmonic oscillations.

[7] Water pressure in the saturated zone was measured with piezometers extending 10 cm into the sand. The piezometers are 5 mm stainless steel tubes perforated with numerous 2.5 mm diameter holes screened by stainless steel mesh with 0.1 mm openings. Measurements were taken visually, by reading ID 8 mm manometer tubes connected to the piezometers with a reading accuracy of ±1 mm.

2.2. Sand

[8] The sand in the flume consists mainly of quartz and is mined locally from Pleistocene coastal dunes. It is well sorted with $d_{50} = 0.20$ mm and $d_{90}/d_{10} = 1.83$, providing a more or less homogeneous medium. In order to avoid trapped air, the sand was added to the flume by allowing it to settle by gravity through clear water, in layers of the order 10 cm thick. The procedure was repeated until the flume was filled to the top with saturated sand, draining the clear water as required. The sand's hydraulic and moisture characteristics were investigated by *Nielsen and Perrochet* [2000] and are presented in Table 1.

[9] The two packing types in Table 1 were dry packed into the column so, as the flume was packed by allowing the sand to settle by gravity though the water-filled flume, the present packing is likely to be a little looser than the loosest of these. For comparison, the hydraulic conductivity, K, was also calculated based on measured sediment characteristics (sieve curve) using the empirical formulation of *Krumbein and Monk* [1942] which gave $K = 0.00053$ m/s. Throughout all of the following analysis the parameters for packing type B in Table 1 have been adopted.

[10] The flume was covered with loose plastic to minimize evaporation and the sand remained moist to the top and the mean water table was 40 cm ($\approx 0.73 H_\psi$) below the sand surface. Possible implications of a truncated capillary fringe are discussed in section 3.3.

2.3. Driving Head

[11] The driving head, $h_o(t)$, was almost sinusoidal,

$$h_o(t) = d + A_o \cos \omega t = d + A_o \Re\left(e^{i\omega t}\right) \quad (1)$$

where d is the mean elevation, A_o is the amplitude and ω ($=2\pi/T$) is the angular frequency. The amplitude of the first and second harmonics were $R_\omega = 0.235$ m and $R_{2\omega} = 7$ mm, respectively, with the ratio $R_{2\omega}/R_\omega \approx 1/34$ confirming the almost simple harmonic nature of the driving head. The period was $T = 772$ s, corresponding to $\omega = 0.0081$ rad/s which falls in the range of infra-gravity and long waves observed in oceans. The vertical accelerations are very small, with $\omega^2 A_o/g \approx 1.6 \times 10^{-6}$, and so the pressure in the clear water reservoir is taken to be hydrostatic. Table 2 provides a summary of the driving head parameters.

[12] Given the above period and using the sand parameters of packing type B listed in the bottom row of Table 1, the present experiment leads to the nondimensional, "coastal"

Table 1. Hydraulic Parameters of the Test Sand[a]

Packing Type	K, m/s	θ_s, vol/vol	θ_r, vol/vol	H_ψ, m
A	0.00015	0.38	0.08	0.60
B	0.00047	0.41	0.09	0.55

[a] K, saturated hydraulic conductivity; θ_s and θ_r, saturated and residual moisture contents, respectively; H_ψ, steady capillary fringe thickness. After *Nielsen and Perrochet* [2000].

Table 2. Summary of Aquifer Forcing Parameters

Parameter	Value
T, s	772
R_ω, m	0.235
$R_{2\omega}$, m	0.007
d, m	1.094

aquifer response number $N_{CAR} = K/n\omega H_\psi = 0.33$ which indicates that capillary fringe effects will be important for this setup [cf. *Li et al.*, 1997]. For comparison, if we consider forcing from a tide of period 12.25 hours (where capillary effects are considered to be small) with the same sand parameters used above, we obtain $N_{CAR} = 18.7$.

[13] Since the data analysis is based on the assumption of a steady oscillation, the flume was left running steadily for at least 24 hours before measurements. This ensured that any start-up transients had disappeared since the timescale for water table adjustments at the "inland" end ($x = 9$ m) is $T_{adj} = |n_e|x^2/(Kd) \approx 2.6$ hours.

3. Observations and Analysis

[14] The observed time series of head oscillations from selected stations along the flume are shown in Figure 2 with the head variation at all stations essentially simple harmonic like the driving head. The amplitude decays exponentially inland and a phase lag grows linearly in accordance with small-amplitude theory,

$$\eta(x,t) = A_o e^{-k_r x}\cos(\omega t - k_i x) = A_o \mathrm{Re}\{e^{-(k_r+ik_i)x}e^{i\omega t}\} \qquad (2)$$

[15] Comparison of the behavior near the base, $z = 0.1$ m (solid symbols) with that closer to the water table $z = 0.8$ m (open symbols) reveals effects of finite aquifer depth.

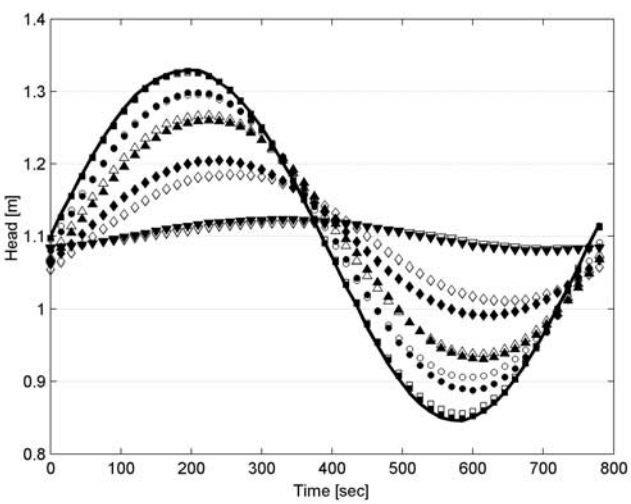

Figure 2. The driving head (solid line) and the piezometric head measured at $z = 0.1$ m (solid symbols) and $z = 0.8$ m (open symbols) at five selected stations along the flume: $x = 0.04$ m (solid and open squares), $x = 0.29$ m (solid and open circles), $x = 0.54$ m (solid and open triangles), $x = 1.34$ m (solid and open diamonds) and $x = 3.34$ m (solid and open inverted triangles).

Closest to the interface at $x = 0.04$ m (solid and open squares), the head at both levels is very similar to that of the driving head, i.e., little damping has occurred and the head is more or less hydrostatic as in the clear water. The slight difference at low tide is believed to be due to seepage face formation. At $x = 0.29$ m (solid and open circles), the heads are hydrostatic except at low water where the level at $z = 0.8$ m sits above that at $z = 0.1$ m. At $x = 0.54$ m (solid and open triangles), the oscillation amplitudes are similar but the mean at $z = 0.8$ m is greater than at $z = 0.1$ m (see section 3.1). At $x = 1.34$ m (solid and open diamonds) we see the finite depth behavior of the amplitude near the bottom (solid symbols) being greatest and the head near the bottom leads that at the top (open symbols).

[16] The latter is consistent with the finite depth theory of *Nielsen et al.* [1997], who by relaxing the hydrostatic pressure assumption, obtained the small-amplitude, expansion solution,

$$h_j^*(x,z,t) = B_j \mathrm{Re}\left\{e^{-k_j x}\frac{\cos k_j z}{\cos k_j d}e^{i\omega t}\right\} \qquad (3)$$

where the subscript $j = 1..\infty$, represents the wave mode and B_j is the amplitude of the piezometric head at $(x, z) = (0, d)$ for the jth wave mode. Equation 3) shows that the pressure (p) distribution due to each mode is nonhydrostatic so a combination of modes is required to match the hydrostatic clear water boundary condition. The nonhydrostatic behavior and higher wave mode boundary condition requirements are discussed in detail in sections 3.4 and 3.5, respectively.

[17] Table 3 summarizes the results (time means, amplitudes and phases) of harmonic analysis conducted on

Table 3. Time Mean Values ($\overline{h^*}$), Amplitudes ($R_{m\omega}$), and Phases ($\phi_{m\omega}$) of the First Two Harmonics (Angular Frequencies ω and 2ω) of the Piezometric Head at Different Points in the Flume

x, m	z, m	$\overline{h^*}$, m	R_ω, m	ϕ_ω, rad	$R_{2\omega}$, m	$\phi_{2\omega}$, rad
0	–	1.094	0.235	0	0.007	0
0.035	0.10	1.094	0.233	0.01	0.006	0.03
0.135	0.10	1.096	0.223	0.05	0.007	0.36
0.29	0.10	1.097	0.200	0.13	0.004	0.76
0.54	0.10	1.098	0.165	0.25	0.003	0.68
0.84	0.10	1.099	0.139	0.24	0.002	0.74
1.34	0.10	1.099	0.106	0.37	0.001	0.82
1.84	0.10	1.100	0.076	0.48	–	–
2.34	0.10	1.100	0.047	0.69	–	–
3.34	0.10	1.101	0.022	1.07	–	–
4.84	0.10	1.099	0.009	1.47	–	–
6.84	0.10	1.099	0.002	2.00	–	–
8.84	0.10	1.099	0.001	2.34	–	–
0	–	–	–	–	–	–
0.035	0.80	1.096	0.229	0.01	0.005	0.00
0.135	0.80	1.099	0.210	0.05	0.001	1.04
0.29	0.80	1.101	0.192	0.10	0.002	2.00
0.54	0.80	1.102	0.163	0.22	0.002	2.49
0.84	0.80	1.101	0.132	0.32	0.001	3.02
1.34	0.80	1.100	0.088	0.53	0.001	2.79
1.84	0.80	1.100	0.058	0.73	–	–
2.34	0.80	1.101	0.039	0.94	–	–
3.34	0.80	1.099	0.019	1.23	–	–
4.84	0.80	1.099	0.008	1.62	–	–
6.84	0.80	1.099	0.003	2.28	–	–
8.84	0.80	1.099	0.001	2.31	–	–

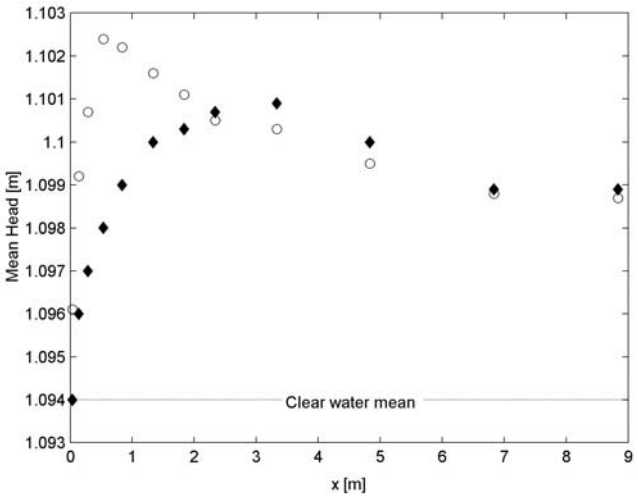

Figure 3. Measured time averaged piezometric heads close to the bottom $\overline{h^*x, 0.1\text{m}}$ (solid diamonds) and close to the water table $\overline{h^*x, 0.8\text{m}}$ (open circles). The mean driving head level is also shown (dashed line).

observations from all piezometers. If the amplitude of the second harmonic $R_{2\omega}(x, z)$ was large enough ($\geq$1 mm), it too was extracted along with the corresponding phase $\phi_{2\omega}$.

3.1. Mean Head Values

[18] The time-averaged head profiles $\overline{h^*(x, 0.1\text{ m})}$ and $\overline{h^*(x, 0.8\text{ m})}$ are shown in Figure 3. At both levels, the piezometric head is higher for $x \rightarrow \infty$ than at $x \rightarrow 0^+$. However, the common asymptotic value, $\overline{h^*_\infty}$, of approximately 1.099 m is below the ''Boussinesq'' value of $\sqrt{d^2 + A_o^2/2} \approx 1.107$ m derived by *Philip* [1973]. In other words, with a mean water level of $d = 1.094$ m in the driving head reservoir, the measured inland over-height was only $\overline{\eta_\infty} = 0.005$ m compared to 0.013 m given by *Philip*'s [1973] shallow aquifer, capillary-free theory.

[19] This difference is interesting because *Philip*'s [1973] result was shown by *Knight* [1981] to be valid even if the aquifer is not shallow. The differences are therefore believed to be due to capillary effects. Recently, *Silliman et al.* [2002]. demonstrated that horizontal as well vertical flows were present in the capillary fringe and this may play a role. However, meniscus suction on the vertical face of the aquifer at $x = 0$ may well be different from that at the inland boundary. If there was no such imbalance, the simple requirement of balance between the total pore water pressure forces at $x = 0$ and at $x = 8.84$ m (where the oscillation has died out),

$$\overline{\int_{z=0}^{sandsurface} p(0, z, t).dz} = \overline{\int_{z=0}^{sandsurface} p(8.84, z, t).dz} \qquad (4)$$

would lead to *Philip*'s [1973] result, i.e., $\overline{h(8.84\text{ m})} = \sqrt{d^2 + A_o^2/2} \approx 1.107$ m. Since the flume was covered with loose plastic and the sand remained moist at the top, evaporation is not believed to have been significant.

[20] Conditions are hydrostatic in the clear water reservoir and below the water table at the landward end, and hence $\overline{h^*}$ does not depend on z at these boundaries. However, in the range $0 < x < 4$ m, we see that the conditions are not hydrostatic as the mean piezometric head is different at the two levels, with values at the top being greater than at the bottom. The pressure in the driving head reservoir at $x = 0$ is hydrostatic but inside the sand, deviations from hydrostatic conditions develop very rapidly to a peak difference of 4 mm between $x = 0.25$ m and $x = 0.5$ m. The fact that both $\overline{h^*(x, 0.1\text{ m})}$ and $\overline{h^*(x, 0.8\text{ m})}$ show local maxima instead of increasing monotonically with x is not covered by any theory known to the writers. S. Dunn et al. (manuscript in preparation, 2003) present a detailed investigation of the observed time-averaged head levels including an analytical solution to describe the resultant circulation.

3.2. Oscillation Amplitudes, Phases, and Wave Numbers

[21] As mentioned previously in section 3, the observed oscillations will at any point contain contributions from several modes. However, the contributions from individual modes cannot be separated on the basis of measurements at a single point so the following analysis will be on the overall signal including all contributions from all modes.

[22] As expected, the time-variation of the piezometric head at each measuring point is essentially simple harmonic,

$$\overline{h^*}(x, z, t) \approx R_\omega(x, z) \cos[\omega t - \phi_\omega(x, z)] \qquad (5)$$

see Table 3. The oscillation amplitudes, $R_\omega(x, z)$, decay in the inland direction and the phase lags, $\phi_\omega(x, z)$, compared with the driving head, increase. These decay rates and phase shift variations with x reflect those of a simple water table-wave of the form (2). That is, an ''overall'' wave number (for the total signal at angular frequency, ω) can be estimated by fitting straight lines to plots of $\ln[A_o/R_\omega(x, z)]$ ($=k_r x$) and phase lag, $\phi_\omega(x, z) - \phi_\omega(0)$ ($=k_i x$). These quantities are plotted in Figure 4.

[23] We see that both $\ln[A_o/R_\omega(x, z)]$ and the phase lags show essentially the linear growth with x that corresponds to a single wave mode of the form (2). Least squares fitting of straight lines lead to, $k = k_r + ik_i = 0.687 + 0.293i$ or, with $d = 1.094$ m,

$$kd = 0.752 + 0.321i \qquad (6)$$

This gives a ratio, $k_r/k_i \approx 2.3$ which is comparable to the values found in the field by *Nielsen* [1990] and *Aseervatham* [1994] for fluctuations at the tidal frequency as described in section 1. If the forcing frequency were that of a tidal signal, capillary effects would be negligible [e.g., *Li et al.*, 1997] so the field values are likely to be dominated by finite depth effects whereas the present experiment has a significant influence from the capillary fringe (see section 2.3). The ''overall'' wave number (equation (6)) will correspond rather closely to the actual wave number of the primary mode because the higher modes decay very rapidly (see section 3.4).

3.2.1. Finite Depth Effects

[24] Under the shallow aquifer assumption of hydrostatic pressure and neglecting capillarity effects, the wave number can be predicted by the ''Boussinesq'' wave number,

$$k = (1 + i)\sqrt{\frac{n\omega}{2Kd}} \qquad (7)$$

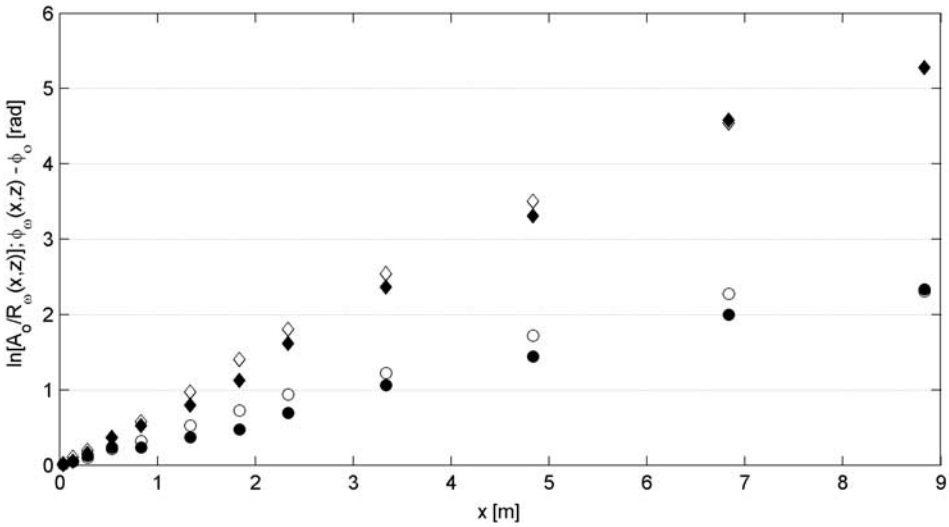

Figure 4. Amplitude decay, $\ln[A_o/R_\omega(x, z)] = k_r x$ (solid and open diamonds), and phase lags, $\phi_\omega(x, z) - \phi_\omega(0) = k_i x$ (solid and open circles) for the fundamental frequency ω plotted as function of distance from the driving head reservoir. Solid symbols correspond to measurements near the bottom ($z = 0.1$ m), while the open symbols correspond to measurements near the water table ($z = 0.8$ m).

where, n is the drainable porosity ($=\theta_s - \theta_r$; θ_s is the saturated moisture content and θ_r is the residual moisture content), ω the angular frequency, K the saturated hydraulic conductivity and d the mean aquifer depth and i is the imaginary unit [see, e.g., *Todd*, 1960]. Using the packing type B sand parameters from Table 1 and the forcing parameters in Table 2, equation (7) predicts,

$$kd = 1.741(1 + i) \tag{8}$$

i.e., $k_r = k_i$ which is clearly not the case for the present experiment.

[25] The dispersion relation (7) only holds for shallow aquifers, i.e., in the limit of negligible dimensionless depth, $n\omega d/K \to 0$. For finite $n\omega d/K$ (i.e., nonhydrostatic pressure), *Nielsen et al.* [1997] derived the following finite depth, small-amplitude dispersion relation,

$$kd \tan kd = i\frac{n\omega d}{K} \tag{9}$$

Note that (7) emerges from (9) when only the first term of the Taylor expansion for tan kd is used. For finite $n\omega d/K$, there are infinitely many wave modes of the form (2) at each frequency because equation (9) has infinitely many complex roots k_j. The real parts ($k_{r,j}$) of these wave numbers increase by approximately π/d from one mode to the next [cf. *Nielsen et al.*, 1997; *Li et al.*, 2000]. This means that, according to equation (2), the higher modes decay very rapidly compared with the primary mode. The imaginary parts ($k_{I,j}$) are however very similar indicating similar speeds of propagation for all modes.

[26] For the present parameters equation (9) predicts,

$$kd = 1.526 + 0.257i \tag{10}$$

The comparison with equation (6) is improved somewhat in terms of the phase (k_i) but the decay rate (k_r) is still too strong.

3.2.2. Capillarity Effects

[27] At higher frequencies, water table oscillations will be influenced by capillarity [e.g., *Li et al.*, 1997; *Nielsen and Perrochet*, 2000]. Under the shallow aquifer assumption (neglecting vertical flow effects), *Barry et al.* [1996] solved a modified Boussinesq equation with the capillarity correction of *Parlange and Brutsaert* [1987] for water table waves described by (2) and obtained the following dispersion relation,

$$k = \sqrt{\frac{n\omega}{2d}\left[\frac{1}{\sqrt{K^2 + (\omega B)^2}} \pm \frac{\omega B}{K^2 + (\omega B)^2}\right]} \tag{11}$$

where $B = nH_\psi$ is the capillary fringe thickness.

[28] For the present parameters, equation (11) predicts,

$$kd = 1.358 + 0.217i \tag{12}$$

thereby reducing the decay rate slightly but still over predicting it in comparison to the observed value, (6).

[29] A useful mathematical technique to account for capillarity effects is to replace the drainable porosity, n, in the dispersion relations (7) and (9) with the complex effective porosity, n_e, defined as

$$\frac{n_e}{n} = \frac{dh_{tot}}{dt} \Big/ \frac{dh}{dt} \tag{13}$$

where h_{tot} is the equivalent height of total drainable moisture and h is the water table height. The complex nature of n_e is such, so as to mathematically account for the damped response of $h_{tot}(t)$ to $h(t)$ through its magnitude, $|n_e|$, and for the phase lag of $h_{tot}(t)$ behind $h(t)$ through its argument, $Arg\{n_e\}$ [*Nielsen and Perrochet*, 2000].

[30] For an oscillating water table, n_e is a function of the dimensionless frequency $n\omega H_\psi/K$. The *Green and Ampt*

[1911] capillary fringe model of a fringe height, H_ψ, with the pressure at the top of the fringe being constant at $-\rho g H_\psi$, leads to [*Nielsen and Turner*, 2000],

$$n_e = \frac{n}{1 + i\frac{n\omega H_\psi}{K}} \tag{14}$$

[31] Equation (14) implies that $|n_e| < n$, so by replacing n with the complex n_e in equations (7) and (9) results in smaller wave numbers which, in turn, leads to a slower damping rate and a faster wave propagation. When substituted into (7), (14) yields the shallow aquifer dispersion relation, (11), as obtained by *Barry et al.* [1996]. When substituted into (9), (14) gives the same finite depth, dispersion relation obtained by *Li et al.* [2000], their equation (7). Using the present parameters, this model [(9) with $n = n_e$ by (14)] predicts,

$$kd = 1.063 + 0.097i \tag{15}$$

An improved decay rate is seen but the speed of propagation is over-predicted.

[32] Following the 1-D sand column experiments of *Nielsen and Perrochet* [2000], *Nielsen and Turner* [2000] proposed a slightly different, but analogous form of n_e via an empirical curve fit to the column data of $n_e(n\omega H_\psi/K)$ for three differing soil types,

$$n_e = \frac{n}{1 + C\left(i\frac{n\omega H_\psi}{K}\right)^{2/3}} \tag{16}$$

where, C is an empirical constant. Taking $C = 2.5$ and the present parameters, this model [(9) with $n = n_e$ by (16)] gives,

$$kd = 0.868 + 0.218i \tag{17}$$

which, though over-predicting both the decay rate and phasing, is seen to provide the best comparison with the experimental value, equation (6), of all the models outlined above.

[33] Comparisons of all the above models with the "overall" best fit wave number (equation (6)) are summarized graphically in Figure 5. The much improved comparison when using the complex effective porosity derived from the empirical formulation, equation (16) (solid squares), is clearly evident.

[34] The sensitivity of all the models outlined above, to the aquifer parameters K (open squares), n (open circles) and H_ψ (open diamonds), is illustrated in Figure 6 where the following range of parameters was tested: K = [0.000235 m/s; 0.00047 m/s; 0.00094 m/s]; n = [0.2; 0.32; 0.4]; H_ψ = [0.4 m; 0.55 m; 0.7 m]. The analysis shows that changes in K and n will shift the wave numbers along the same dispersion relation curve, whereas a change in H_ψ will shift the whole curve closer or further from the origin. Of all the models, the finite depth with the empirical capillary fringe model (equation (9) with n_e by equation (16)) is seen to be the least sensitive as a consequence of the 2/3 power in the denominator of equation (16) as opposed to the power of 1 in equation (14).

3.3. Effective Porosity

[35] The effective porosity applicable to the present sand parameters and wave frequency can be found by inserting the experimental value, equation (6), for kd on the left-hand side of equation (9) and solving for n (= n_e), leading to,

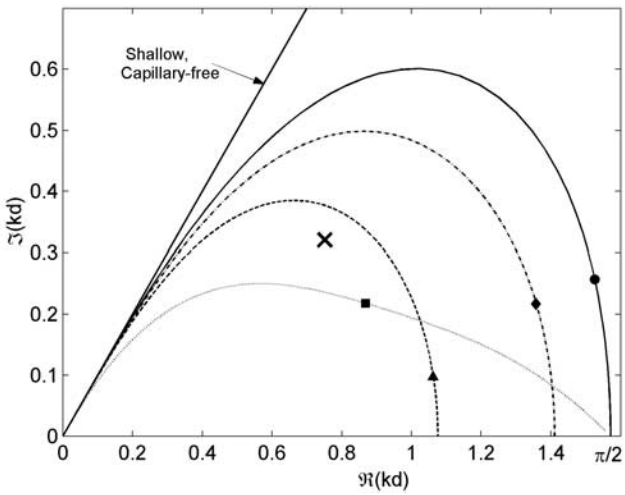

Figure 5. Comparison of the overall, best fit wave number equation (6) (cross) with those predicted by the finite depth dispersion relation, equation (9), using a real valued porosity (solid circle), and complex effective porosities as defined by equations (14) (solid triangle) and equation (16) (solid square). The shallow aquifer, with capillary fringe value defined by equation (11) is also shown (solid diamond). The associated curves illustrate the wave dispersion properties for $0 < n\omega d/K < \infty$ for each of the above models. Parameters used are T = 772 s; d = 1.094 m; n = 0.32; K = 0.00047 m/s; H_ψ = 0.55 m.

$$n_e = 0.034 - 0.022i \tag{18}$$

which gives $|n_e| = 0.041$ and $\mathrm{Arg}\{n_e\} = -0.57$ radians (=33°). Parameters used are: T = 772 s, d = 1.094 m, n = 0.32, K = 0.00047 m/s, H_ψ = 0.55 m.

[36] As discussed in section 3.2, the necessary n_e, as defined by equation (13), is complex in nature to mathematically account for the fact that the total moisture lags behind the water table. The (negative) argument of n_e gives the phase angle which describes this lag and given the present forcing period of 772 s, the 33° phase angle corresponds to the total moisture lagging behind the water table by 70 s. The best fit n_e value, equation (18), is shown in Figure 7 (crosses), together with values obtained for the same sand in column experiments as described by *Nielsen and Perrochet* [2000]. For comparison, the effective porosity based on the *Green and Ampt* [1911] model, equation (14), is also plotted and the discrepancy between this model and data is clearly apparent.

[37] The implications of such an effective porosity to natural systems can be discussed by returning to the definition of n_e given by equation (13). Taking the magnitude of the experimental value, $|n_e| = 0.041$, equation (13) states that for the present forcing and aquifer parameters (n = 0.32), a 10 cm change in water table height will result in only a 1.3 cm change in total moisture. Thus the presence of a capillary fringe will limit moisture exchange due to high frequency water table waves [*Nielsen and Turner*, 2000]. An example environment where this is important is

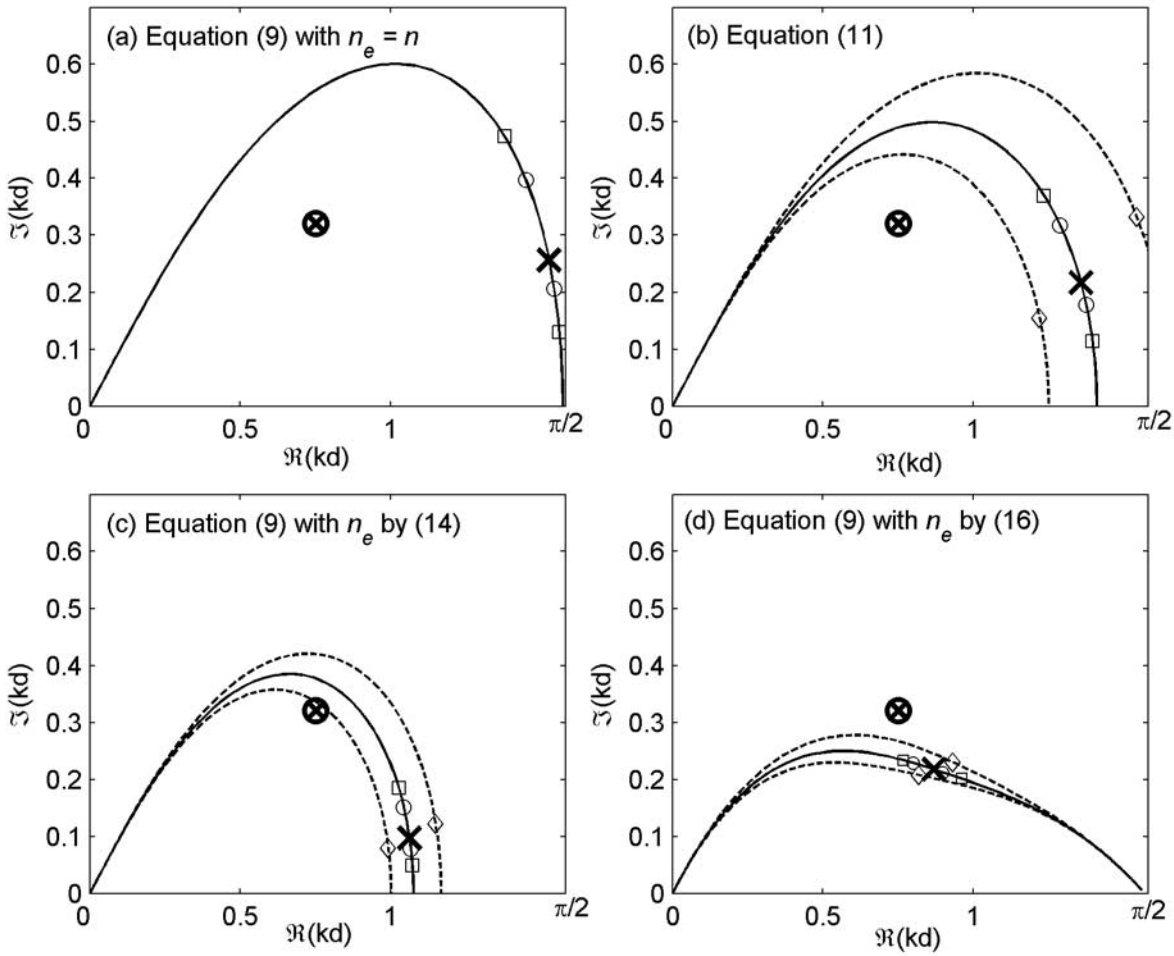

Figure 6. Sensitivity of theoretical dispersion relations to variations in the aquifer parameters, K (open squares), n (open circles), and H_ψ (open diamonds). The points shown correspond to the range of parameters: K = [0.000235 m/s; 0.00094 m/s]; n = [0.2; 0.4]; H_ψ = [0.4 m; 0.7 m]. Circled crosses denote the experimental value, and crosses denote the theoretical predictions based on the experimental parameters: T = 772 s; d = 1.094 m; n = 0.32; K = 0.00047 m/s; H_ψ = 0.55 m.

the wave run-up zone on beaches where the forcing free water waves have periods ranging from around 10 s for wind waves to the order of minutes for long waves. Equations (14) and (16) indicate that this effect becomes more important at higher frequencies.

[38] The effective porosities calculated using the *Green and Ampt* [1911] equation (14), and the empirical formulation (16), are $n_e = 0.031 - 0.095i$ and $n_e = 0.043 - 0.051i$ respectively. The fact that these values (calculated using theory and experiments under a fully developed fringe) are slightly greater than the "best fit" value (equation (18)) could, in part, be related to the fact that in the present experiment the capillary fringe was truncated (see section 2.2). Column experiments on oscillating water tables under a truncated capillary fringe indicate that the complex effective porosity is reduced compared to that obtained under a fully developed fringe (pluses and stars in Figure 7). The implication of this on the propagation of a water table wave may be qualitatively described on inspection of the dispersion relations (7) and (9). If n_e is reduced due to a truncated fringe, then smaller wave numbers will result and hence less damping and an increase in wave speed. This phenomenon could have important implications for high frequency oscillations in beaches where, just landward of the shoreline, the water table lies just below the sand surface. The effect of a truncated fringe in the present experiments, however, is considered minor as the present experimental value (crosses) shown in Figure 7 is within the range of scatter in the column data obtained under a fully developed capillary fringe.

3.4. Nonhydrostatic Behavior

[39] At the interface with the clear water reservoir, at $x = 0$, conditions must be hydrostatic. Hence oscillation amplitudes and phase shifts are observed to be practically identical at the top and at the bottom of the aquifer for x = 0.04 m (see Figure 2 and Table 3). However, both oscillation amplitudes and phases display clear nonhydrostatic features in the interior. That is, for $x > 1$ m, the oscillation amplitudes R_ω and $R_{2\omega}$ are larger at the bottom than at the top (see Table 3). This is in qualitative agreement with the small-amplitude, finite depth theory of *Nielsen et al.* [1997], as expressed by equation (3). The theory

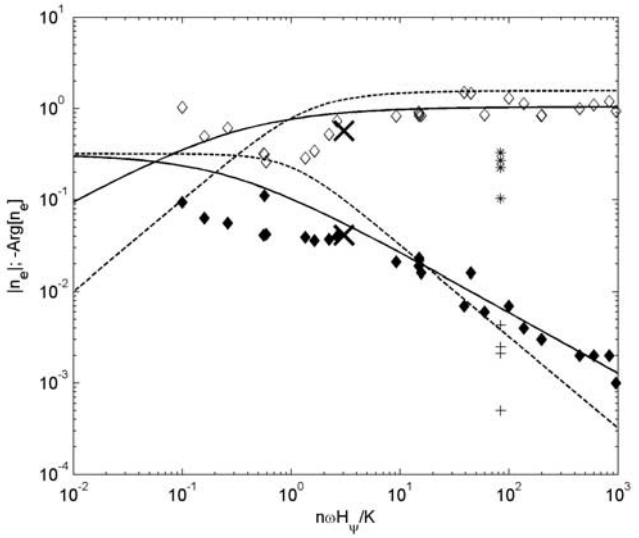

Figure 7. The best fit effective porosity obtained by inserting equation (6) into equation (9) is shown in terms of its magnitude $|n_e|$, and argument $-\mathrm{Arg}\{n_e\}$ (both shown as crosses) and compared with values obtained with the same sand used in the column experiments by *Nielsen and Perrochet* [2000a, 2000b]. The solid symbols diamonds indicate $|n_e|$, and the open symbols diamonds indicate $-\mathrm{Arg}\{n_e\}$. The curves are calculated using equations (14) (dashed lines) and (16) with $C = 2.5$ (solid lines). The stars and pluses indicate data collected under a truncated capillary fringe, with pluses and stars representing $|n_e|$ and $-\mathrm{Arg}\{n_e\}$, respectively.

predicts different ratios, $R_{\omega,j}(x, 0.1\text{ m})/R_{\omega,j}(x, 0.8\text{ m})$, for the different modes at each frequency and the overall behavior corresponds to a linear combination of several modes. However, the primary mode dominates for $x > 1$ m because the higher modes decay very rapidly due to their much larger k_r values, see Table 4.

[40] The primary mode with wave number $k_{\omega,1}$ taken as the overall best fit value, corresponding to equation (6), gives the head amplitude ratio $R_\omega(x, 0.1\text{ m})/R_\omega(x, 0.8\text{ m})$,

$$\frac{\cos(k_{\omega,1} \times 0.1\text{ m})}{\cos(k_{\omega,1} \times 0.8\text{ m})} = 1.117 + 0.155i = 1.13e^{0.14i} \qquad (19)$$

i.e., a magnitude ratio of 1.13 and a phase lead of the head at $z = 0.1$ m by 0.14 radians.

[41] The data, which contains contributions from all modes, show considerable variation as seen for $x < 1$ m in Figure 8. However, for $x > 1$ m where the higher modes are insignificant, there is reasonable agreement. Thus the nonhydrostatic behavior displayed landward of the decay of the higher modes is in agreement with small-amplitude theory. Also comforting is the much improved agreement upon inclusion of capillarity effects via both equations (14) (dash-dotted line) and (16) (solid line).

3.5. Multiple Mode Content Due to the Hydrostatic Boundary Condition at $x = 0$

[42] The pressure distribution in the clear water reservoir at $x = 0$ is hydrostatic. However, the individual water table wave modes all have a nonhydrostatic pressure distribution given by (3) which corresponds to,

$$h^*_{\omega,j}(x, z, t) = h^*_{\omega,j}(x, 0, t)\cos k_{\omega,j} z \qquad (20)$$

where $k_{\omega,j}$ with $j = 1, 2, \ldots\infty$, are the infinitely many roots of the dispersion relation (9). This means that an expansion solution, i.e., a combination of modes is needed in order to match a hydrostatic boundary condition like,

$$h^*(0, z, t) = d + A_o \cos\omega t = d + \mathrm{Re}\{A_o e^{i\omega t}\} \quad , \quad 0 < z < d \qquad (21)$$

We follow the notation of *Nielsen et al.* [1997] and write the piezometric head as an expansion of the form,

$$h^*(x, z, t) = d + \mathrm{Re}\left\{A_o e^{i\omega t}\sum_{j=1}^{\infty} A_{\omega,j} e^{-k_{\omega,j}x}\cos k_{\omega,j} z\right\} \qquad (22)$$

which for $x = 0$ becomes,

$$h^*(0, z, t) = d + \mathrm{Re}\left\{A_o e^{i\omega t}\sum_{j=1}^{\infty} A_{\omega,j}\cos k_{\omega,j} z\right\} \qquad (23)$$

which means that the head coefficients, $A_{\omega,j}$, for the different modes are determined from,

$$1 = \sum_{j=1}^{\infty} A_{\omega,j}\cos k_{\omega,j} z \text{ for } 0 < z < d \qquad (24)$$

[43] The values corresponding to the present experiment for $A_{\omega,j}$, which gives the mode contribution at $(x, z) = (0, 0)$, along with the coefficient $B_{\omega,j} = A_{\omega,j}\cos k_{\omega,j} d$, which gives the mode contribution at $(x, z) = (0, d)$, are given in Table 4. The alternating behavior of $A_{\omega,j}$ is typical (see Table 1 of *Nielsen et al.* [1997]) and is seen to converge quite rapidly with respect to the head at the bottom, $B_{\omega,j}$. Hence the convergence of the expansion is slower near the water table than at the bottom.

[44] The way in which the successive approximations, including more and more modes in equations (22)–(24), approach the constant (hydrostatic) head over the range $0 < z < d$ at $x = 0$, is illustrated by Figure 9 with the parameter values for the present experiment, corresponding to the

Table 4. Wave Numbers in Terms of the Dimensionless Depths $k_{\omega,j}d$ ($d = 1.094$ m) and Head Coefficients for $z = 0$ ($A_{\omega,j}$) and at $z = d$ ($B_{\omega,j}$) Based on the $k_{\omega,1}d$ Equal to the Overall Best Fit Value Equation (6) and the Small-Amplitude Theory of *Nielsen et al.* [1997]

j	$k_{\omega,j}d$	$A_{\omega,j}$	$B_{\omega,j}$
1	$0.752 + 0.321i$	$1.079 + 0.078i$	$0.846 - 0.181i$
2	$3.283 + 0.190i$	$-0.094 - 0.100i$	$0.098 + 0.098i$
3	$6.351 + 0.102i$	$0.022 + 0.031i$	$0.022 + 0.031i$
4	$9.469 + 0.069i$	$-0.010 - 0.014i$	$0.010 + 0.014i$
5	$12.600 + 0.052i$	$0.005 + 0.008i$	$0.005 + 0.008i$
6	$15.734 + 0.042i$	$-0.003 - 0.005i$	$0.003 + 0.005i$
7	$18.872 + 0.035i$	$0.002 + 0.004i$	$0.002 + 0.004i$
8	$22.010 + 0.030i$	$-0.002 - 0.003i$	$0.002 + 0.003i$
Sum		$0.999 - 0.001i$	$0.989 - 0.018i$

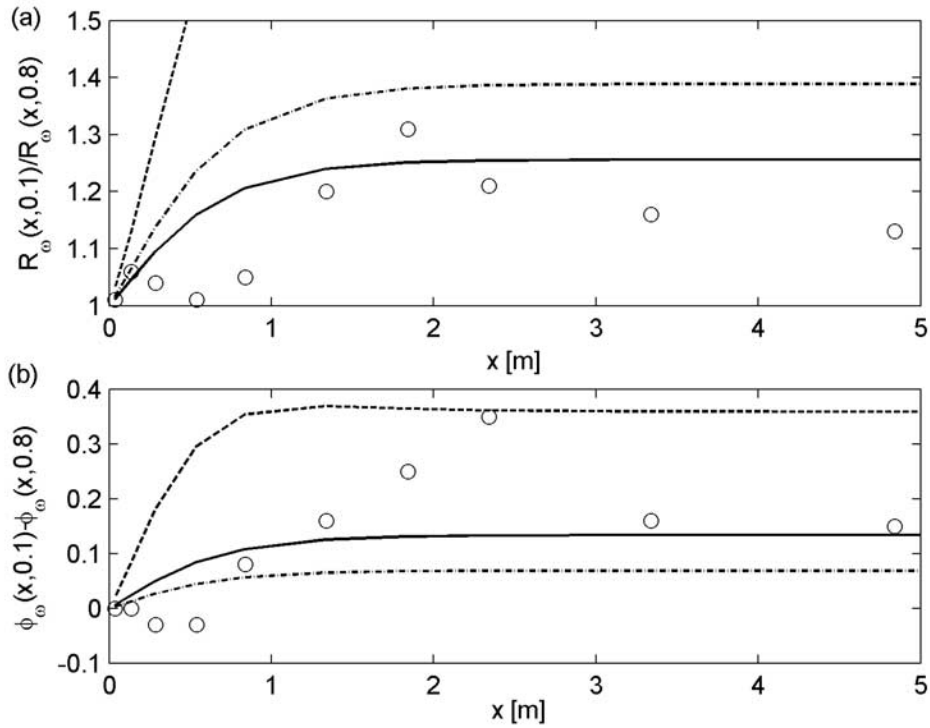

Figure 8. Comparison of (a) measured (open circles) amplitude ratios and (b) phase leads with those obtained by equation (3). Theoretical wave numbers were calculated using the dispersion relation (9) with a real valued porosity (dashed lines), and the complex effective porosities by equations (14) (dash-dotted lines) and (16) (solid lines). Parameters used are T = 772 s; d = 1.094 m; n = 0.32; K = 0.00047 m/s; H_ψ = 0.55 m.

coefficients $A_{\omega,j}$ and $B_{\omega,j}$ in Table 4. We see that the convergence of equation (24) is much faster at $z = 0$ than at $z = d$. The expansion solution (24), being part of a small-amplitude solution, exact only for $A_o/d \rightarrow 0$, has limited meaning above $z = d$.

[45] The solution, equation (3), solves, in part, the problem of matching the hydrostatic clear water reservoir with the nonhydrostatic pressure field in the interior as outlined by *Dagan* [1967]. This is achieved by matching the hydrostatic boundary condition with a suitable combination of nonhydrostatic modes in the interior. However, the small-amplitude expansion, equation (3), is only applicable over the range $0 < z < d$ and therefore neglects the water pressure between $z = d$ and the water surface at maximum driving head level. It also neglects any meniscus suction above $z = d$ at minimum driving head level. The modeling of these aspects requires a finite amplitude formulation of the boundary condition and consideration of capillary suction at the vertical interface, including seepage face dynamics. Such a boundary condition is so far not available in a form suited for analytical solution. Hopefully, the experimental findings of the present study can assist in the process of achieving this.

[46] Capillary suction and a possible seepage face will complicate the boundary condition at $x = 0$ in the way qualitatively outlined in Figure 10. The fact that the complete small-amplitude solution contains many modes, each decaying with x at different rates, suggests that the overall decay of the head oscillations is not necessarily exponential and that the overall phase shift may not necessarily grow linearly with x, i.e., the data points in Figure 4 should not necessarily fall along straight lines. This is illustrated in Figure 11 where we have zoomed in to the first 3 m only and the phase of the driving head has been subtracted from the local phase angles. The multiple-mode

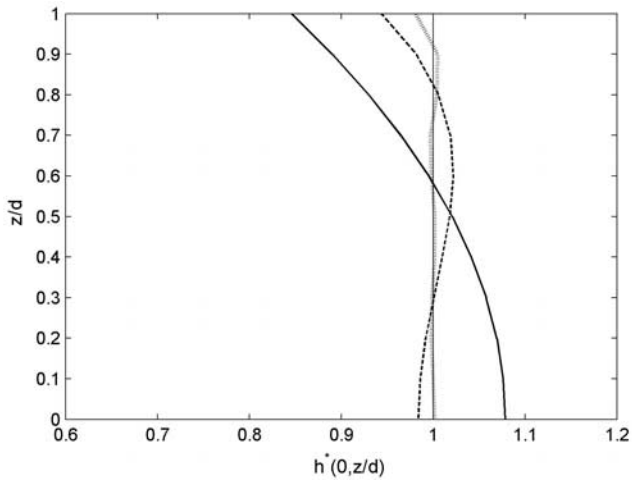

Figure 9. Dimensionless head amplitude at $x = 0$, $h^*(0, z/d)$, given by equation (24), including the primary mode only (solid line), the first two modes (long-dashed line) and the first five modes (short-dashed line).

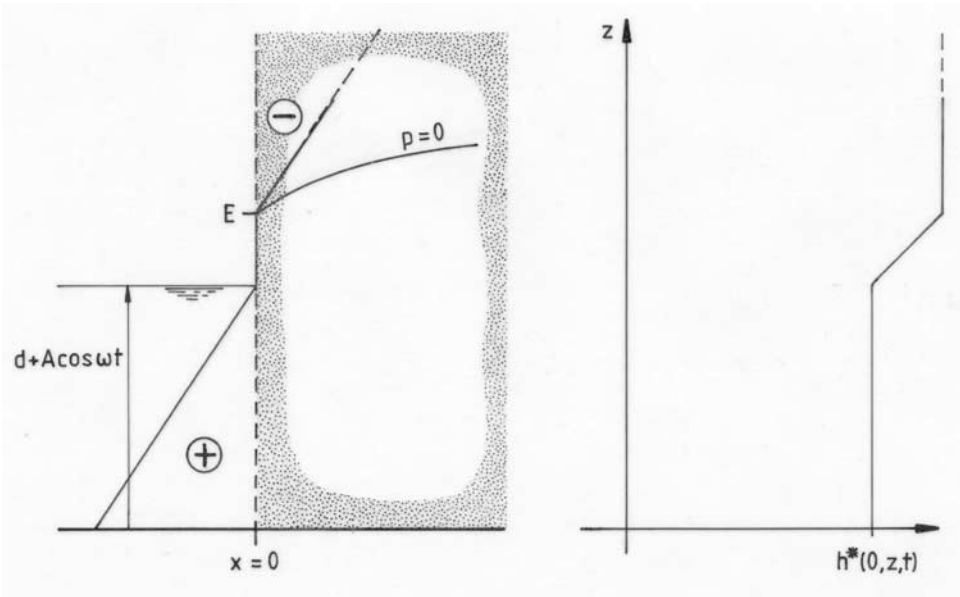

Figure 10. At low water a seepage face may form between the driver level and the moving exit point E, along which, the pressure is atmospheric. Hence $h^* = p/\rho g + z$ will increase linearly between the surface and E. Above E the pore pressure may again be hydrostatic and h^* constant up to a height comparable with H_ψ above E. The appearance of a seepage face is seen to increase the time-mean head at $x = 0$ and hence throughout. The variation of the seepage face height through the forcing cycle might be expected to drive higher harmonic components of h^* in the aquifer. However, in this study such higher harmonics were found to be insignificant.

theory near the bottom, (solid lines), show a slight downward convex trend while closer to the top, (dashed lines), an upward convex behavior is seen. As in Figure 8 the comparison in the transitional, multiple-mode zone, $0 < x < 1$ m, is not so good.

[47] By definition, the lines and the symbols in Figure 11 all come together at the origin. The lines then diverge and become parallel for $x > 1$ m indicating that only the primary mode remains. The asymptotic distance between the upper lines corresponds to the amplitude ratio $R_{\omega,1}(x, 0.1\text{ m})/R_{\omega,1}(x, 0.8\text{ m}) = 1.13$ calculated from equation (19). The asymptotic distance between the lower lines corresponds to the phase lead of 0.14 radians (7.9°) by $h^*_{\omega,1}(x, 0.1\text{ m})$ ahead of $h^*_{\omega,1}(x, 0.8\text{ m})$.

[48] The differences between each set of symbols and the corresponding line in Figure 11 are, of course, partly due to measurement scatter. However, the differences may also indicate ''theoretical'' differences, i.e., the differences that would exist between perfect measurements and the expansion solution (22) which is derived from a simplified boundary condition as discussed in connection with Figures 9 and 10.

3.6. Higher Harmonics

[49] If a seepage face forms during part of the forcing cycle (see Figure 10), the $h^*(0, z, t)$ variation at points above $z = d$ will not necessarily be simple harmonic. Hence the seepage face will probably generate higher harmonic components of $h^*(x, z, t)$ near $x = 0$. It is also conceivable that other nonlinear phenomena could generate higher harmonics. However, the second harmonics measured in our experiment were everywhere equal to or smaller than that in the driving head reservoir (see Table 3 with $R_{2\omega}(0) = 7$ mm). In other words, the measured second harmonics do not indicate that seepage face formation or any other phenomenon generated significant second harmonic oscillations at $x = 0$.

[50] A number of researchers [*Steggewentz*, 1933; *Dagan*, 1967; *Parlange et al.*, 1984] have investigated the generation of higher harmonics in the interior due to

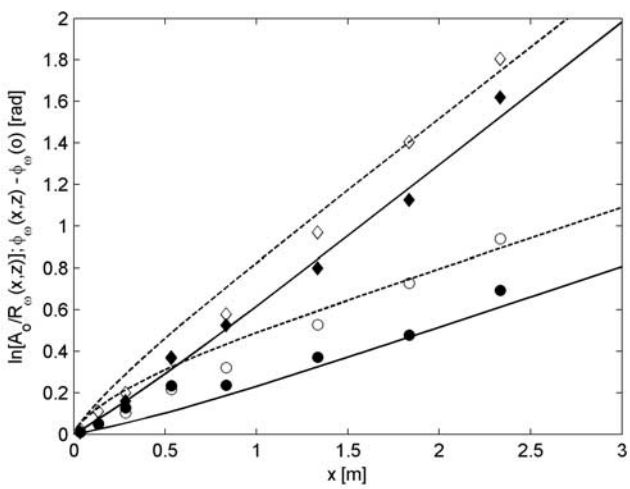

Figure 11. Details of the h^* oscillation decay measured by $\ln[A_o/R_\omega(x, z)]$ and phase lags, $\phi_\omega(x, z) - \phi_\omega(0)$, over the first 3 m of the flume. Symbols shown represent phase lag at $z = 0.1$ m (solid circles) and at $z = 0.8$ m (open circles); $\ln[A_o/R_\omega(x, z)]$ at $z = 0.1$ m (solid diamonds) and at $z = 0.8$ m (open diamonds). For each symbol the nearest line shows the same quantity according to the small-amplitude expansion (equation (22)).

nonlinearity of the field equation. They carried out the analysis for shallow aquifers with no capillary effects and found that due to the nonlinearity of the Boussinesq equation a simple harmonic wave at frequency ω and wave number k will generate two waves at frequency 2ω, one that decays as $\exp(-\sqrt{2}k_r x)$ and one that decays as $\exp(-2k_r x)$. These two, 2ω-modes cancel each other at $x = 0$ but yield a maximum amplitude of approximately $0.179A_o^2/d$ for $kx \approx 0.6$ which, for our experiment, corresponds to a maximum amplitude of 5 mm between $x = 0.5$ m and $x = 1$ m. Our experimental data show essentially a monotonic decay of $R_{2\omega}$ from the driving head value of 7 mm at $x = 0$. Hence the generation of second harmonics by nonlinearity in the interior seems to have been weakened by the presence of a capillary fringe in our experiment. All in all, the present finite amplitude ($A_o/d \approx 0.22$) experiments show no evidence of significant second harmonics being generated at the interface or in the interior.

4. Conclusions

[51] Detailed measurements of the piezometric head $h^*(x, z, t)$ have been performed in a nonshallow ($|n_e\omega d/K| \approx 6$) sand flume interacting with a hydrostatic clear water reservoir through a vertical interface at a frequency where capillary effects are significant.

[52] The h^* oscillations display approximately exponential decay and linearly growing phase lag relative to the driving head, which is predicted by shallow aquifer, small-amplitude, capillarity free theory. However, significant differences were observed which are most easily summarized in terms of the wave numbers for the corresponding water table waves. That is, decay rates and phase shifts in the simple theory correspond to wave numbers with equal real and imaginary part ($k_i = k_r$), while the best fit wave number (equation (6)) for the overall behavior of the measurements gives $k_r/k_i \approx 2.3$. This difference is due partly to finite aquifer depth $|n_e\omega d/K| \approx 6$ and partly to capillary fringe effects, $H_\psi/d \approx 0.38$.

[53] Comparison of wave number prediction using the dispersion relations (7) and (9) with the experimental estimate (equation (6)), is greatly improved upon inclusion of capillary effects via the complex effective porosity concept of *Nielsen and Perrochet* [2000] (see Figure 5). The best comparison is obtained using the finite depth dispersion relation (9), with the empirical complex effective porosity (equation (16)). This model is also shown to be the least sensitive to variations in the aquifer parameters, K, n and H_ψ (see Figure 6).

[54] Applied in a quasi-predictive manner (i.e., using the experimental wave number, equation (6), as input), the small-amplitude theory of *Nielsen et al.* [1997] (equation (3)) appropriately accounts for the observed finite depth effects of greater amplitude and phase lead at the base. Using the best fit wave number (equation (6)) and the finite depth dispersion relation (equation (9)), a best fit value of n_e is obtained and agrees closely with those obtained from 1-D vertical sand column experiments with the same sand, as reported by *Nielsen and Turner* [2000] (see Figure 7).

[55] The h^* oscillations far from the driving head reservoir ($x > 1$ m) have greater amplitude near the bottom than near the water table $|h^*(x, 0.1\text{ m}, t)|/|h^*(x, 0.8\text{ m}, t)| \approx 1.13$ and the oscillations at the bottom lead those close to the water table by about 0.14 radians. This is in agreement with the finite depth, small-amplitude theory of *Nielsen et al.* [1997] as described by equation (3).

[56] The transition from the multiple mode hydrostatic behavior near the driving head reservoir ($x \rightarrow 0^+$) to the asymptotic single mode behavior for $x > 1$ m is qualitatively modeled by small-amplitude theory. However, the observed differences in the details of this transition (Figure 11), between the small-amplitude solution and the measurements, are probably more than measurement scatter. We expect that upwards from the present value ($A_o/d = 0.22$) a more detailed finite amplitude formulation of the boundary condition is warranted.

[57] The mean water table height is higher for $x \rightarrow \infty$ than for $x \rightarrow 0^+$ in qualitative agreement with the shallow aquifer theories of *Philip* [1973] and *Parlange et al.* [1984]. However, the rise in mean head levels is not monotonic as predicted by these theories, a maximum occurs at about $x = 1$ m (see Figure 3). The asymptotic inland over-height is only about 1/3 of the shallow, capillary free aquifer value. This reduction may not be entirely due to nonshallowness. Differences in the time-averaged capillary suction patterns at the two ends of the aquifer may also play a role. The time-mean piezometric head $\overline{h^*(x,z)}$ is significantly nonhydrostatic in the range $0.04\text{ m} < x < 2.5$ m with larger values at the top indicating steady downward flow in the upper part of the aquifer.

[58] Nonlinear effects were surprisingly small in the experiments with no evidence of second harmonics being generated either by the finite amplitude ($A_o/d = 0.22$) boundary condition or by nonlinearity in the interior.

Notation

A_o	amplitude of (simple harmonic) driving head, m.
$A_{\omega,j}$	amplitude of piezometric head fluctuation at (0,0), m.
B	capillary fringe thickness = nH_ψ, m.
$B_{\omega,j}$	amplitude of piezometric head fluctuation at (0,d), m.
d	time averaged driving head level, m.
d_{50}	median sediment size, mm.
$\phi_{m\omega}$	harmonic phase, radians.
g	acceleration due to gravity, m/s^2.
h_o	driving head level, m.
h	water table elevation, m.
h^*	piezometric head level, m.
$\overline{h^*}$	time-averaged piezometric head level, m.
h_{tot}	equivalent height of total moisture, m.
H_ψ	equivalent, steady capillary fringe height, m.
i	imaginary unit.
j	wave mode component.
k	wave number = $k_r + ik_i$, rad/m.
k_r	amplitude decay rate, rad/m.
k_i	rate of increase of phase lag, rad/m.
k_j	wave mode wave number, rad/m.
K	saturated hydraulic conductivity, m/s.
m	harmonic component.
n	drainable porosity.
n_e	(complex) effective porosity.
η	water table fluctuation, m.
$\overline{\eta_\infty}$	asymptotic inland water table overheight, m.
θ_s	saturated moisture content.
θ_r	residual moisture content.
$R_{m\omega}$	harmonic amplitude, m.

$R_{\omega,j}$ amplitude of wave mode, m.
ρ density of fluid, kg/m^3.
x shore-normal coordinate, m.
t time, s.
T period, s.
ω angular frequency, rad/s.
z vertical coordinate, m.

[59] **Acknowledgments.** The present research work has been supported by the Collaborative Research Centre (CRC) for Sustainable Tourism as project number 52001. The support of an Australian Postgraduate Award for the first author is also acknowledged. The authors also acknowledge the valuable comments received during the review process.

References

Aseervatham, A. M., Tidal dynamics of coastal watertables, Ph.D. thesis, 253 pp., Univ. of Queensland, Brisbane, Australia, 1994.

Barry, D. A., S. J. Barry, and J.-Y. Parlange, Capillarity correction to periodic solutions of the shallow flow approximation, in *Mixing in Estuaries and Coastal Seas, Coastal Estuarine Stud.*, vol. 50, edited by C. B. Pattiaratchi, pp. 496–510., AGU, Washington, D. C., 1996.

Dagan, G., Second-order theory of shallow free-surface flow in porous media, *Q. J. Mech. Appl. Math.*, *20*(4), 517–526, 1967.

Green, W. H., and G. A. Ampt, Studies on soil physics I. The flow of air and water through soils, *J. Agric. Sci.*, *4*, 1–24, 1911.

Kang, H.-Y., A. M. Aseervatham, and P. Nielsen, Field measurements of waverunup and the beach watertable, *Rep. CE148*, 44 pp., Dep. of Civ. Eng., Univ. of Queensland, Brisbane, Australia, 1994.

Knight, J. H., Steady periodic flow through a rectangular dam, *Water Resour. Res.*, *17*(4), 1222–1224, 1981.

Krumbein, W. C., and G. D. Monk, Permeability as a function of the size parameters of unconsolidated sand., *Am. Inst. Min. Metall. Eng. Tech. Publ.*, *11*,11 pp., 1942.

Li, L., D. A. Barry, J.-Y. Parlange, and C. B. Pattiaratchi, Beach water table fluctuations due to wave run-up: Capillarity effects, *Water Resour. Res.*, *33*(5), 935–945, 1997.

Li, L., D. A. Barry, F. Stagnitti, and J.-Y. Parlange, Groundwater wave in a coastal aquifer: A new governing equation including vertical effects and capillarity, *Water Resour. Res.*, *36*(2), 411–420, 2000.

Nielsen, P., Tidal dynamics of the water table in beaches, *Water Resour. Res.*, *26*(9), 2127–2134, 1990.

Nielsen, P., and P. Perrochet, Watertable dynamics under capillary fringes: Experiments and modelling, *Adv. Water Resour.*, *23*(1), 503–515, 2000. (Errata, *Adv. Water Resour.*, *23*, 907–908, 2000.)

Nielsen, P., and I. Turner, Groundwater waves and water exchange in beaches, paper presented at 27th International Conference on Coastal Engineering, Am. Soc. of Civ. Eng., Sydney, Australia, 2000.

Nielsen, P., A. M. Aseervatham, J. D. Fenton, and P. Perrochet, Groundwater waves in aquifers of intermediate depths, *Adv. Water Resour.*, *20*(1), 37–43, 1997.

Philip, J. R., Periodic non-linear diffusion: An integral relation and its physical consequences, *Aust. J. Phys.*, *26*, 513–519, 1973.

Parlange, J.-Y., and W. Brutsaert, A capillarity correction for free surface flow of groundwater, *Water Resour. Res.*, *23*(5), 805–808, 1987.

Parlange, J.-Y., F. Stagnitti, J. L. Starr, and R. D. Braddock, Free-surface flow in porous media and periodic solution of the shallow-flow approximation, *J. Hydrol.*, *70*, 251–263, 1984.

Raubenheimer, B., R. T. Guza, and S. Elgar, Tidal water table fluctuations in a sandy ocean beach, *Water Resour. Res.*, *35*(8), 2313–2320, 1999.

Silliman, S. E., B. Berkowitz, J. Simunek, and M. T. van Genuchten, Fluid flow and solute migration within the capillary fringe, *Ground Water*, *40*(1), 76–84, 2002.

Steggenwentz, J. H., The influence of the tidal motion of seas and tidal rivers on the height of rise of groundwater (in Dutch), Ph.D. thesis, 138 pp., Delft Univ. of Technol., Delft, Netherlands, 1933.

Todd, D. K., *Ground Water Hydrology*, 336 pp., 2nd ed., John Wiley, Hoboken, N. J., 1960.

N. Cartwright and P. Nielsen, Division of Civil Engineering, School of Engineering, University of Queensland, St. Lucia, 4072 Queensland, Australia. (nick.cartwright@uq.edu.au; p.nielsen@uq.edu.au)

S. Dunn, HR Wallingford Ltd, Howbery Park, Wallingford OX10 8BA, UK. (s.dunn@hrwallingford.co.uk)